Design of Highly Efficient Catalyst for Rational Way of Direct Conversion of Methane

I.Z. Ismagilov[1*], E.V. Matus[1], M.A. Kerzhentsev[1], I.P. Prosvirin[1], R.M. Navarro[2], J.L.G. Fierro[2], G. Gerritsen[3], E. Abbenhuis[3], Z.R. Ismagilov[1,4]

[1]Boreskov Institute of Catalysis SB RAS, pr. Akademika Lavrentieva 5, 630090 Novosibirsk, Russia
[2]Instituto de Catálisis y Petroleoquímica, CSIC, Marie Curie 2, 28049 Madrid, Spain
[3]Hybrid Catalysis B.V., Den Dolech 2, Eindhoven 5612, AZ, the Netherlands
[4]Institute of Coal Chemistry and Material Science SB RAS, pr. Sovetskiy 18, 650000 Kemerovo, Russia

Article info

Received:
21 October 2014
Received and revised form:
29 December 2014
Accepted:
18 February 2015

Abstract

Effects of composition and preparation method of $MnNaW/SiO_2$ and LaSr/CaO catalysts on their physical-chemical properties and performance in oxidative coupling of methane (OCM) have been studied. For $MnNaW/SiO_2$ catalysts the synthesis method and type of SiO_2 have a significant effect on the texture, while the Na/W ratio determines the phase composition. The variation of preparation method and temperature of catalyst calcination allows regulation of the metal surface concentration and mode of metal distribution across the SiO_2 support. For LaSr/CaO catalysts the synthesis method determines the specific surface area, surface and phase composition. Correlations between catalyst performance, preparation method and state of the catalyst were established. The rational preparation procedure and perspective composition of OCM catalyst have been developed. The 20La/CaO catalysts prepared by citrate sol-gel method were shown to provide ~20% C_2 yield and ~40% methane conversion at 800 ºC.

1. Introduction

Design of highly efficient catalyst for rational way of conversion of methane will solve such problems as effective utilization of natural gas and environmental protection [1-7]. The production of C_2 hydrocarbons (i.e. ethylene + ethane) through the oxidative coupling of methane (OCM) is an attractive direct way of the natural gas utilization into the value added products (Eqs. (1), (2)):

$$2CH_4 + 0.5O_2 \rightarrow C_2H_6 + H_2O \quad (1)$$

$$C_2H_6 + 0.5O_2 \rightarrow C_2H_4 + H_2O \quad (2)$$

Although considerable efforts have been placed on the search of commercially suitable OCM catalyst, the C_2 yield is still less than the 30% threshold for practical application [2, 8, 9]. The limit of C_2 yield is connected with the thermodynamically favoured nonselective oxidation of hydrocarbons to CO and CO_2. According to the OCM reaction mechanism [8, 10, 11], the active surface species play a key role in the methyl radical formation. The radicals should recombine selectively to ethane, which is then dehydrogenated to ethylene oxidatively. Methoxy species formed on the surface or in the gas phase finally react to carbon dioxide. The reduction of gaseous oxygen concentration can provide the increase of selectivity of C_2 formation [10].

Many different reactor concepts were proposed to improve the C_2 yield such as fixed bed reactor, fluidized bed reactor, porous and dense membrane reactors, solid oxide fuel cell reactor [12, 13]. It was demonstrated that membrane reactor exhibits appreciable advantages over traditional packed bed reactor [14-16]. The most significant potential of membrane reactor in OCM process is its ability to increase the C_2 selectivity by controlling of the oxygen addition. In recent years, a great deal of effort has been directed towards OCM with the use of mixed ionic-electronic conducting membranes (MIECM membranes), but only a few examples demonstrated a C_2 yield higher than 30% [14-16].

* Corresponding author. E-mail: zinfer1@mail.ru

It was postulated that for the further enhancement of C_2 yield in membrane reactor, efficient catalyst systems should be provided and the development of a high permeation flux MIEC membrane alone is not a sufficient strategy for the successful industrial implementation of an OCM membrane reactor [16]. In addition, the kinetic compatibility requires a good match between oxygen permeation rate and reaction rate as crucial for OCM reaction [14]. Thus the goal of this study is creation of an efficient catalyst for OCM to be used in catalytic membrane reactor (CMR). $MnNaW/SiO_2$ and LaSr/CaO type catalysts were shown to be among the most suitable for this purpose, and therefore we have undertaken a systematic synthesis, physicochemical and catalytic characterization study of a series of such compositions and their modifications, with a perspective of their integration into the CMR. These studies will be applied to understand the structure-property-performance relationships and elucidate crucial factors, variation of which at the stage of catalyst preparation allows regulation of the OCM reaction parameters.

2. Experimental

2.1 Catalyst preparation

The series of OCM catalysts were synthesized by different preparation routes. The abbreviation in the bracket indicates the preparation method: (I) is the incipient wetness impregnation method, (M) is the mixture slurry method, (S) is the sol-gel method and (PM) is physical mixing. The number in the sample formula indicates the nominal metal content (wt.%). The $MnNaW/SiO_2$ (I) catalysts were prepared by sequential incipient wetness impregnation method. At first a SiO_2 support was impregnated by an aqueous solution of sodium tungstate dihydrate $Na_2WO_4{\cdot}2H_2O$ and sodium oxalate $Na_2C_2O_4$ taken in an appropriate amounts. Then NaW/SiO_2 was dried at 120 ºC for 6 h and impregnated by an aqueous solution of manganese acetate tetrahydrate $Mn(CH_3COO)_2{\cdot}4H_2O$ taken in an appropriate concentration. The catalysts were then dried at 120 ºC for 6 h and calcined in air at 850 ºC for 6 h. The nature of the SiO_2 substrate was varied and the main characteristics of SiO_2 sources are presented in Table 1.

The modification of $MnNaW/SiO_2$ (I) catalyst by Ce, La, Zr, Cl, P or S was performed [17]. In this case the corresponding metal precursor of promoter (cerium nitrate $Ce(NO_3)_3{\cdot}6H_2O$, lanthanum nitrate $La(NO_3)_3{\cdot}6H_2O$, oxychloride of zirconium $ZrOCl_2{\cdot}8H_2O$, sodium sulphate Na_2SO_4, sodium thiosulphate $Na_2S_2O_3$, disodium hydrogen phosphate $Na_2HPO_4{\cdot}12H_2O$, monosodium phosphate $NaH_2PO_4{\cdot}2H_2O$, sodium chloride NaCl) was added into the impregnating solution. The SiO_2-3 silica was used for this series of catalysts.

The $MnNaW/SiO_2$ (M) catalysts were prepared by the mixture slurry method. Aqueous solutions of salts (manganese acetate tetrahydrate $Mn(CH_3COO)_2{\cdot}4H_2O$, sodium tungstate dihydrate $Na_2WO_4{\cdot}2H_2O$, sodium oxalate $Na_2C_2O_4$) taken in appropriate concentrations were added dropwise to silica sol (SiO_2-5, Table 1) with stirring, and the mixture was agitated vigorously for several hours. The mixture slurry was dried at 120 ºC for 6 h and calcined in air at 850 for 6 h.

The LaSr/CaO (S) catalysts were prepared by citrate sol-gel method. Aqueous solutions of salts (lanthanum nitrate $La(NO_3)_3{\cdot}6H_2O$, strontium nitrate $Sr(NO_3)_2$, calcium nitrate $Ca(NO_3)_2{\cdot}4H_2O$) taken in a required ratio were added to a solution of citric acid (CA) at 60 ºC. The reagents were used in molar ratio (La + Ca + Sr) : CA = 1 : 1. Then this mixture was kept at 60 ºC for the time required to form a highly viscous gel, which was dried at 100 ºC and then self-ignited producing a dry powder. The obtained product was dried at 120 ºC and then calcined in air at 850 ºC for 6 h.

LaSr/CaO (PM) catalysts were prepared by physical mixing of nitrate metal salts (lanthanum nitrate $La(NO_3)_3{\cdot}6H_2O$, calcium nitrate $Ca(NO_3)_2{\cdot}4H_2O$, strontium nitrate $Sr(NO_3)_2$) taken in a required ratio. The obtained product was dried at 120 ºC and then calcined in air at 850 ºC for 6 h.

Table 1
Characteristics of the SiO_2 source

Sample	Description	Textural data			XRD data
		S_{BET}, m^2/g	V_{pore}, cm^3/g	D_{pore}, nm	
SiO_2-1	custom-made (hydrolysis of TEOS at 50 ºC)	56	0.31	22.0	amorphous SiO_2
SiO_2-2	commercial Silica gel 60, Merck	274	0.71	10.3	
SiO_2-3	commercial Silica gel Davisil 646	323	1.13	14.1	
SiO_2-4	commercial Silica Si 4-5P, Akzo	393	1.03	10.5	
SiO_2-5	sol LUDOX LS, 30 wt.% SiO_2, Sigma-Aldrich	particle size of sol 8-20 nm			-

2.2. Characterization of catalysts

The chemical composition of the prepared catalysts was determined by X-ray fluorescence spectroscopy (XFS) using an ARL analyzer with a Rh anode of an X-ray tube and inductively coupled plasma-atomic emission spectrometry (ICP-AES) method.

BET surface area (S_{BET}), pore volume (V_{pore}) and average pore diameter (D_{pore}) of the supports and catalysts were determined in a Micromeritics ASAP 2400 instrument using N_2 adsorption at -196 ºC. Prior to surface area determination, the powders were degassed under vacuum (10^{-5} mbar) at 423 ºC for 4 h.

The phase composition was determined by X-ray diffraction (XRD) in a 2-theta range of 10-80º in an HZG-4C (Freiberger Prazisionmechanik) diffractometer with a CoK_α (λ = 1.59021 Å) radiation source and a graphite monochromator. Phases were identified using the JCPDF database.

Transmission electron microscopy (TEM) measurements were realized in a high-resolution JEOL JEM-2010 microscope operating at 200 kV with a structural resolution of 0.14 nm. The samples were deposited on perforated carbon supports attached to copper grids. The local elemental analysis of the samples was performed by an energy dispersive X-ray analysis (EDX) method using an EDAX spectrometer equipped with a Si (Li) detector with a resolution of 130 eV.

X-ray photoelectron spectra (XPS) were recorded in a SPECS spectrometer (Germany) using a hemispherical PHOIBOS-150-MCD-9 analyzer (AlK_α radiation, hυ = 1486.6 eV). The binding energy (BE) scale was pre-calibrated using the positions of the peaks of $Au4f_{7/2}$ (BE = 84.0 eV) and $Cu_2p_{3/2}$ (BE = 932.67 eV) core levels. The samples in the form of small granules were loaded onto a conducting double-sided copper scotch. The Si2p peak of SiO_2 catalyst support at 103.3 eV was used to correct charge effects on the sample. Survey spectra were recorded at an analyzer pass energy of 50 eV, and high resolution narrow energy windows at 20 eV. The atomic concentration ratios of elements on the catalyst surface were calculated from the integral photoelectron peak intensities (Mn2p, W4f, Na1s, O1s, C1s, Si2s), which were corrected with theoretical sensitivity factors based on the Scofield's photo-ionization cross sections [18].

2.3. Catalytic activity tests

OCM experiments were performed in a 14 mm i.d. quartz fixed-bed reactor with a feed composition of CH_4 : O_2 : He equal to 4 : 1 : 2 under atmospheric pressure, at temperatures 650-950 ºC and gas flow rate 175 ml_n/min. The gas purity was 99.95% CH_4, 99.995% O_2 and 99.995% He. Prior to each activity test, the catalysts were calcined in an O_2 flow (100 ml_n/min) at 700 ºC for 2 h. In order to minimize the catalyst overheating, the 500 mg sample (fraction of 0.25–0.50 mm) was diluted with an equal amount of SiC. Analysis of both inlet and outlet reaction mixtures were accomplished using a Stanford Research Systems QMS 300 mass spectrometric gas analyzer.

Calculation of the reaction parameters was performed from mass flows considering the change of the reaction volume, which can be determined from the change of He concentration. Selectivity to the reaction products (C_2H_6, C_2H_4, CO and CO_2) was determined using flow rates of products after the reactor. Yield of products was calculated as selectivity multiplied by methane conversion.

3. Results and Discussion

3.1. OCM tests

The results of OCM tests of a wide set of catalysts shows that precise regulation of product yields can be achieved by appropriate variation of catalyst preparation conditions (Figs. 1-5). As follows from Fig. 1, catalyst composition has some effect on C_2 yield. The C_2 hydrocarbons yield tends to increase when i) silica with initial specific surface area 300 m^2/g is used; ii) Mn content is decreased from 3 to 2 wt.%; iii) Na_2WO_4 content is increased from 3 to 5-7 wt.%; iv) the Na/W molar ratio is increased from 1 to 2 (Fig. 1a). The variation of Na content and preparation mode has a more obvious influence on C_2 yield value (Fig. 1b). It can be varied in the range of 6-15%. The mixture slurry method provides formation of more active OCM materials at Na content less than 1.5 wt.%, while the impregnation method have an advantage at Na content above 1.5%. This is probably connected with particularity of crystallization and polymorphic transformations of different sources of SiO_2 (amorphous SiO_2 powder (I) and SiO_2 sol (M)) that leads to different phase composition and texture characteristics of catalysts, as well as behaviour of metal distribution across support, red-ox properties of supported species and metal-support interaction.

The C_2 product yield in the OCM reaction over MnNaW-X/SiO_2 catalysts was strongly affected by the type and content of the promoter X [17]. Among all promoters (X = La, Ce, Zr, S, P, Cl) only Cl introduction leads to notable improvement of catalyst performance and shifts the maximum of C_2 yield to low-temperature region (Fig. 2). However this catalyst shows unstable performance under a durability test in the OCM reaction (Fig. 3). The modification of MnNaW/SiO_2 samples by La (2-5 wt.%) or Ce

(2 wt.%) only slightly influences the activity but improves the stability of the catalyst during the durability test in the OCM reaction (Fig. 3). On the contrary, at modification by Zr (0.3-3.3 wt.%) catalyst performance goes down (Fig. 2a): the methane conversion and C_2 yield decrease from 35 to 6-30% and from 15 to 2-10%, respectively. The S or P introduction also leads to a considerable decrease of both C_2 yield and C_2 selectivity – generally at the expense of a decrease of C_2H_4 formation (Fig. 2b).

Literature data on the stability of the MnNaW/SiO_2 catalyst under OCM reaction conditions are very contradictory [19-26]. In particular, it was found that the catalyst retained its initial activity for a long time (20–97 [19–21], 450 [23], or 500 h [22]). On the contrary, according to data [24–26], the yield of C_2 hydrocarbons began to decrease even after 14 h OCM reaction. The main reasons for decreasing OCM process characteristics with time are the following: a change in the phase composition of the catalyst under the action of a reaction mixture the loss of an active component or a redistribution of the active component between the surface and the bulk of a support, and agglomeration [24, 26, 27]. It was postulated that the deactivation of the MnNaW/SiO_2 catalyst upon its treatment with methane was caused by the reduction of Mn ions [11, 28, 29].

For the modified 2Mn1.6Na3W/SiO_2 catalysts it is obvious that the formation of additional phases containing modifier elements (both individual and combined with the basic components) can change the concentration of surface oxygen-containing centres, which are active in the methane activation [17]. In particular, the improvement of OCM process characteristics in the presence of Cl-modified samples (Fig. 2b) can be explained by increase in the concentration of active sites because of the formation of metal oxyhalides or chlorides and a decrease in the concentration of deep oxidation sites [30]. However in course of OCM reaction the removal of chlorine due to a reaction with water occurs which seems to cause the instability of 2Mn1.6Na3W-1Cl/SiO_2 performance in the long-term test (Fig. 3). It is proposed that stable OCM process performance in the presence of 2Mn1.6Na3W-2La/SiO_2 catalyst is connected with the formation of difficult-to-reduce compounds (La–Mn–Si-O and La–W–O) and the retention of the surface chemical composition of the catalyst upon a long-term exposure to a reaction atmosphere [17].

(a)

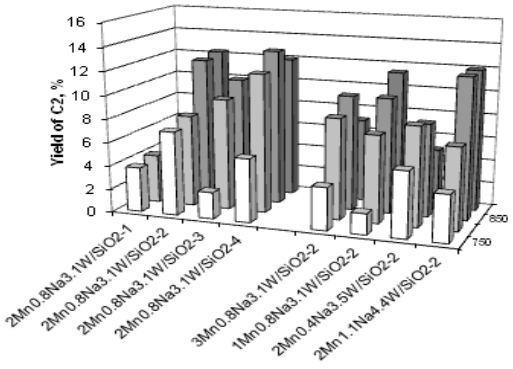

(b)

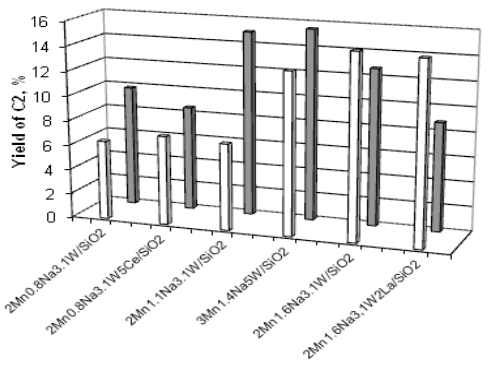

Fig.1. Effect of SiO_2 source, metal content and preparation mode of MnNaW/SiO_2 catalysts on C_2 yield in the OCM reaction.

(a)

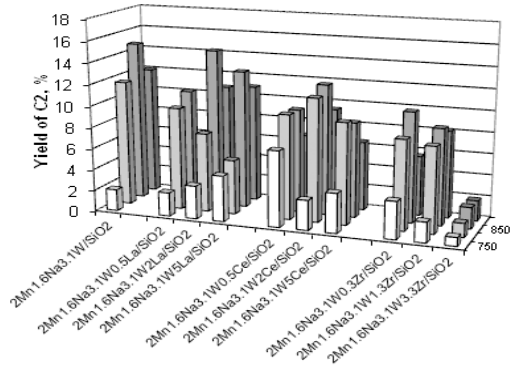

(b)

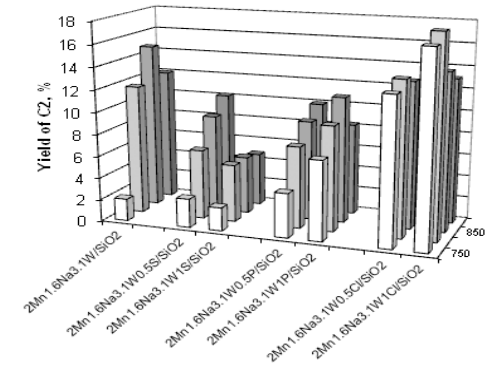

Fig. 2. Effect of type and content of promoter X in 2Mn1.6Na3W-X/SiO_2 catalysts on C_2 yield in the OCM reaction.

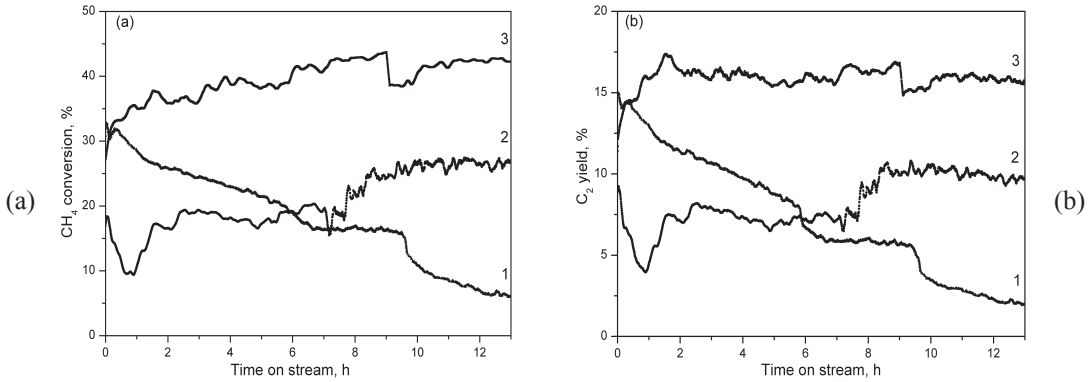

Fig. 3. Effect of catalysts composition on their performance in OCM of CH_4 at 850 ºC. (a) methane conversion vs. time on stream; (b) C_2 yield vs. time on stream. Catalyst composition: (1) – 2Mn1.6Na3W/SiO_2, (2) – 2Mn1.6Na3W-1Cl/SiO_2, (3) – 2Mn1.6Na3W-2La/SiO_2.

Figure 4 shows the effect of the calcination temperature of 2Mn1.6Na3W-2La/SiO_2 catalyst on its activity in the OCM reaction. The methane conversion and C_2 yield increase with an increase of the calcination temperature from 800 to 850 ºC. The further increase of calcination temperature up to 1000 ºC leads to worsening of catalyst performance that can be connected with changes of phase and surface compositions of catalyst. The values of C_2 production selectivity are similar (45-50%) for all samples of this series.

Figure 5 shows the results of a study of the catalytic activity of LaSr/CaO catalysts. It is evident that the conversion of methane increased as the reaction temperature was increased from 600 to 800 ºC, and it insignificantly decreased upon a further increase in the temperature. The C_2 yield increased with the reaction temperature (a maximum at 800 ºC) and then began to lower. The yield of reaction by-products ($CO + CO_2$) increased with the reaction temperature in the entire test range. The observed temperature dependences of OCM reaction characteristics are consistent with previously obtained data, and they reflect the special features of the homogeneous–heterogeneous mechanism of this reaction [30, 31].

The catalytic performance of LaSr/CaO samples is also strongly affected by the chemical composition. The methane conversion increases from 25 to 41%, C_2 yield increases from 11 to 19%, molar ratio C_2H_4/C_2H_6 increases from 0.3 to 0.5 in following order: 20Sr/CaO (S) < 15La-15Sr/CaO (S) < 20La/CaO (S) (Fig. 5). The values of selectivity of C_2 formation for these samples change in the same mode at T < 800 ºC, their values are the same (~45%) at T = 800 ºC. At temperature T > 800 ºC the values of selectivity of C_2 formation increase in the opposite order. The methane conversion increases from 29 to 41%, C_2 yield – from 14 to 19% when the sol-gel method of preparation instead of physical mixing is used (Fig. 5).

The comparison of LaSr/CaO and MnNaW/SiO_2 catalytic systems represented by their best samples (20La/CaO (S) and 2Mn1.6Na3W/SiO_2 (I)) shows that a more wide temperature range of high catalyst performance is provided by the 20La/CaO (S) catalyst (Fig. 6).

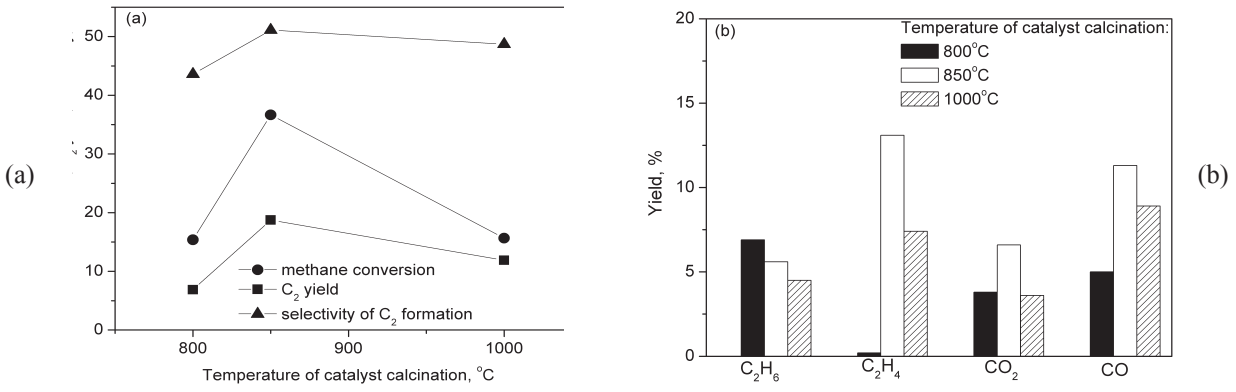

Fig. 4. Effect of temperature of catalyst calcination on the activity of 2Mn1.6Na3W-2La/SiO_2 catalyst in OCM reaction.

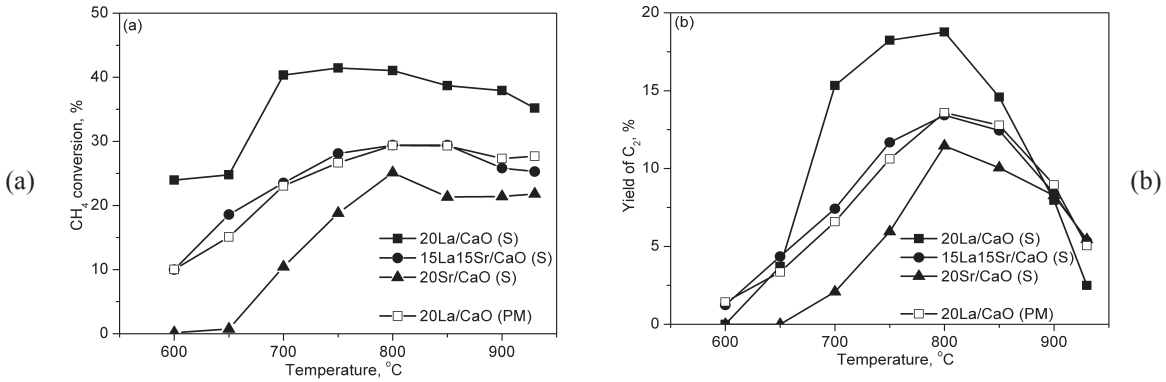

Fig. 5. Effect of chemical composition and preparation mode on activity of LaSr/CaO catalysts in the OCM reaction.

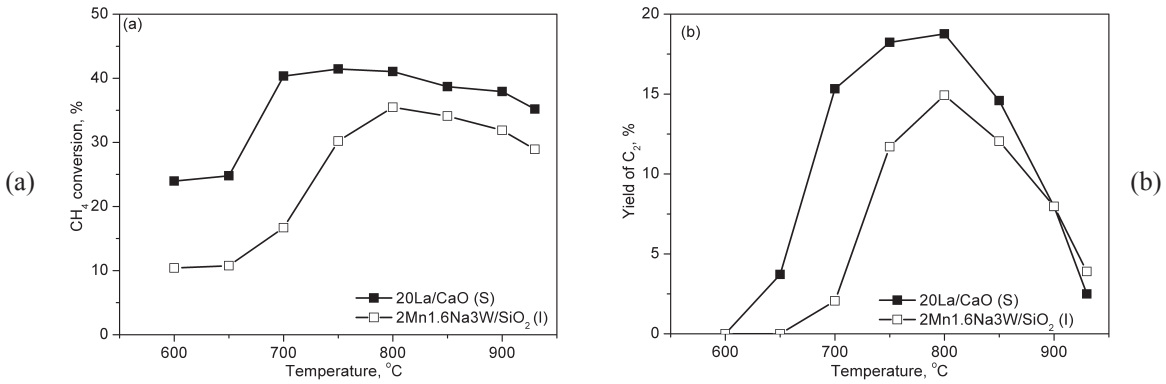

Fig. 6. Performance in the OCM reaction: La/CaO vs. $MnNaW/SiO_2$ catalytic system.

Thus it is shown that the catalyst performance in the OCM reaction can be regulated by catalyst composition, calcination temperature and preparation method of catalyst. Further improvement of OCM reaction parameters can be achieved by variation of reaction conditions. As an example, effects of space velocity and O_2/CH_4 ratio on the C_2 product yields by OCM are presented in Table 2. It is shown that optimal reaction conditions to achieve the maximum efficiency in the C_2 products formation in the OCM reaction are the following: the temperature is 850 ºC; the O_2/CH_4 ratio is 0.25 – 0.375; the gas space velocity is 175 ml/min·g. The $2Mn1.6Na3W/SiO_2$-3 (I) catalyst under optimal reaction conditions provides C_2 hydrocarbons yield of 23.5% and 41% methane conversion at 850 ºC. These values are comparable with or better than those recently reported [2, 8].

Table 2
Effect of space velocity and O_2/CH_4 ratio on OCM reaction parameters on $2Mn1.6Na3W/SiO_2$-3 (I) at 850 ºC.

Catalyst loading, g	Gas space velocity, mL/min·g	O_2/CH_4 ratio	Reaction parameters		
			C_2H_6 yield, %	C_2H_4 yield, %	C_2 yield, %
0.5	350	0.25	6.9	11.0	17.9
1.0	175	0.25	9.0	14.5	23.5
1.5	117	0.25	7.0	9.2	16.2
0.5	175	0.125	5.4	3.4	8.8
0.5	175	0.375	6.1	12.1	18.2
0.5	175	0.50	4.1	10.3	14.4

3.2. Characterization of OCM catalysts

3.2.1. MnNaW/SiO$_2$

The detailed characterization of the studied catalysts was performed by ICP-AES, XRF, N_2 adsorption, XRD, HRTEM-EDX and XPS techniques. It can be noted that in all cases the chemical composition of samples is in good agreement with calculated values. The differences between the nominal and experimental metal content are less than 10% (Table 3).

The addition of metal components to silica followed by calcination at 850 ºC leads to a considerable decrease of specific surface area (from 320 to 1-3 m^2/g), pore volume (from 1.1 to 0.002-0.006 cm^3/g) and average pore diameter (from 14.1 to 6.2-12.7 nm) of support SiO_2 (Tables 2 and 3). It can be explained by the transition of amorphous silica into α-cristobalite and tridymite phases during the calcination.

As follows from Table 3, some increase of specific surface area (from 1.0-1.4 to 2.5-2.9 m^2/g) and pore volume (from 0.002 to 0.007 cm^3/g) occurs with i) application of silica support with high specific surface area (300-400 m^2/g) or ii) decrease of metal content.

As it can be seen from Fig. 7, modification of MnNaW/SiO_2 by different modifying additives leads to some variation of S_{BET}, behaviour of which depends on the type and content of promoter X [17]. It was established that some increase of specific surface area (from 0.8 to 1.2-2.9 m^2/g) and pore volume (from 0.002 to 0.006 cm^3/g) occurred upon the addition of La, Ce or Zr cationic promoters. This effect is more pronounced for the Zr additive in comparison with the La and Ce additives and, probably, connected with the presence of different anions in the salt-precursors. The surface area of the catalysts also increased (up to 2-4 times) with the addition of S or Cl anionic promoter, but P additive has practically no effect on S_{BET} value.

Table 3
Effect of SiO_2 source and metal content on textural properties of MnNaW/SiO_2 catalysts

Sample	Chemical composition, wt.%			S_{BET}, m^2/g	V_{pore}, cm^3/g	Average pore diameter, Å
	Na	W	Mn			
Effect of support						
2Mn0.8Na3W/SiO_2-1	0.8	3.3	1.9	1.0	0.002	90
2Mn0.8Na3W/SiO_2-2	0.9	3.2	2.0	2.6	0.007	110
2Mn0.8Na3W/SiO_2-3	0.9	3.5	2.1	1.7	0.004	85
2Mn0.8Na3W/SiO_2-4	0.8	3.3	2.0	2.5	0.005	75
Effect of Mn content						
1Mn0.8Na3W/SiO_2-2	0.9	3.5	1.2	2.5	0.006	95
3Mn0.8Na3W/SiO_2-2	0.9	3.4	3.2	1.4	0.006	165
Effect of Na_2WO_4 content						
2Mn0.5Na2W/SiO_2-2	0.5	2.0	2.1	2.9	0.008	110
2Mn1.1Na4W/SiO_2-2	1.0	4.4	2.1	2.0	0.005	95
Effect of Na content						
2Mn1.1Na3W/SiO_2-3	1.2	2.8	1.8	1.5	0.003	85
2Mn1.6Na3W/SiO_2-3	1.6	3.5	2.2	0.8	0.002	85

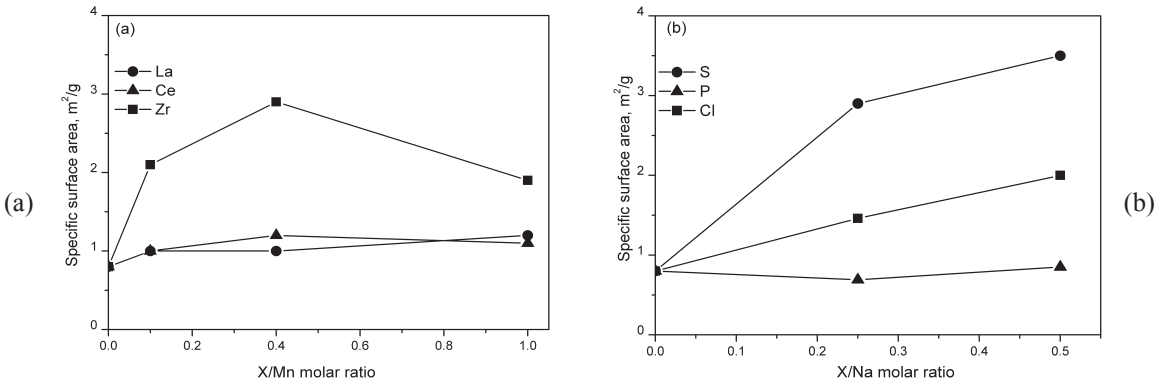

Fig. 7. Effect of X/Mn molar ratio (X = La, Ce, Zr) (a) and X/Na molar ratio (X = S, P, Cl) (b) on S_{BET} of MnNaW-X/SiO_2 catalysts. Calcination temperature is 850 ºC.

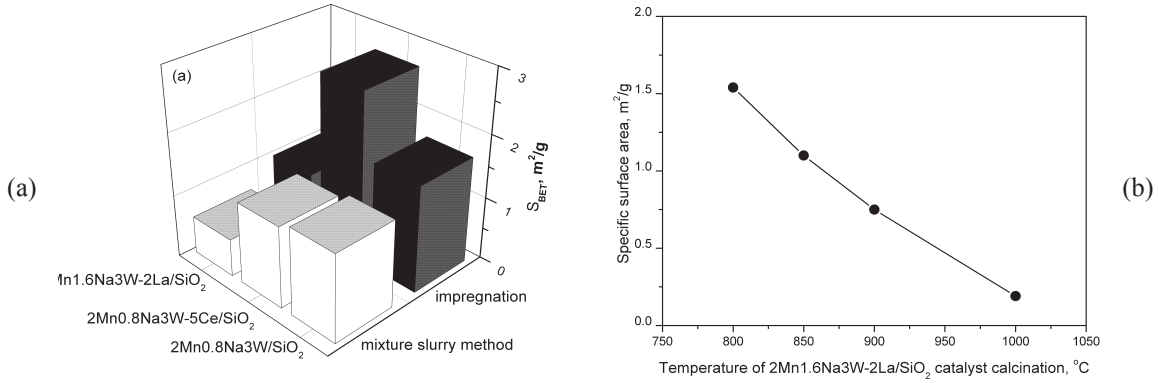

Fig. 8. Effect of preparation mode (a) and calcination temperature (b) of catalysts on their specific surface area.

Figure 8 illustrates the effect of the preparation mode and temperature of catalyst calcination on the catalyst texture. As a rule, the use of the mixture slurry method instead of impregnation leads to lower value of S_{BET}. The specific surface area decreases from 1.5 to 0.2 m^2/g at an increase of calcination temperature from 800 to 1000 ºC.

Because of the low pore volume (~ 0.002-0.005 cm^3/g) and specific surface area (~ 1-3 m^2/g) of MnNaW-X/SiO_2, S_{BET} is mainly related to their external surfaces. It can be suggested that dopant can act as a crystallite growth inhibitor for the silica-based materials, while an increase of calcination temperature leads to crystal sintering. Another reason of S_{BET} variation is different phase compositions of samples (Figs. 9-11).

The α-cristobalite (2θ = 25.6º, 33.2º, 36.7º, 42.2º and other, JCPDS 39-1425), tridymite (2θ = 24.1º, 27.1º, 35,2º, JCPDS 42-1401), Na_2WO_4 (2θ = 19.5º, 32.2º, 37.9º, 50.6 and 61.3º, JCPDS 12-0772) and Mn_2O_3 (2θ = 38.5º, 65.1º, JCPDS 41-1442) phases are observed in the non-modified MnNaW/SiO_2 catalyst after calcination at 850 ºC. The content of phases depends on the chemical composition of the samples. The Na_2WO_4 phase content increases with an increase of Na_2WO_4 content from 3 to 7 wt.% or an increase of Na/W from 1.0 to 2.0. An increase of Mn content from 1 to 3 wt.% or a decrease of Na content from 2 to 0.8 wt.% lead to an increase of Mn_2O_3 phase content.

An increase of Na content as well as an increase of temperature of catalyst calcination lead to an increase of tridymite phase content (Fig. 9). The effect of variation of silica type or preparation techniques on the phase composition of MnNaW/SiO_2 catalysts is insignificant. However the contents of different SiO_2 polymorphic forms (tridymite/α-cristobalite ratio) depend on the preparation mode. At equal content of Na the content of tridymite phase is higher in case of materials prepared by the mixture slurry method in comparison with samples prepared by the impregnation method (Fig. 9a).

Figure 10 shows XRD pattern of 2Mn1.6Na3W/SiO_2 catalyst modified by cationic (Fig.10a) and anionic (Fig. 10b) promoters. At introduction of promoters (La, Ce, Zr, P, Cl), phases which are observed in non-modified samples (α-cristobalite, tridymite, Na_2WO_4 and Mn_2O_3) generally remain and formation of additional phases also takes place [17]. In case of La, the formation of La_2O_3 and $La(OH)_3$ phases is observed. In case of Ce additive, the CeO_2 phase was detected (Fig. 10). For Ce-modified samples, the Mn_2O_3 phase presence is masked by line superposition from CeO_2. The content of CeO_2 phase increases when the content of Ce is increased from 0.5 to 5 wt.% in MnNaW-Ce/SiO_2. In case of Zr additive, the unidentified phase with lines at 2θ = 27.5º, 33.7º, 39.4º, 44.1º, 48.6º and 60.5º was detected in all studied Zr-containing samples. This phase is also observed in Cl-modified samples (Fig. 10b). It can be supposed that formation of this phase is induced by the presence of Cl anions in the material. The source of Cl in the Zr-modified catalysts is $ZrOCl_2 \cdot 8H_2O$ reagent which is used for the preparation of MnNaW-Zr/SiO_2 catalysts. In addition, in the MnNaW-Zr/SiO_2 catalyst with the highest Zr content (3.3 wt.%) an unidentified phase with lines at 2θ = 31.4º and 35.2º was found (Fig. 10a). Probably it is associated with formation of some Zr-containing phase. In case of P additive the Na_3PO_4 phase is found in all prepared MnNaW-P/SiO_2 samples. It is noted that intensity of lines of the Na_3PO_4 phase in diffraction pattern grows with a growth of P content, which may be due to an increase of Na_3PO_4 phase content. A different behaviour is observed in case of S additive. In particular, the presence of the highest content of S additive (~1 wt.%) leads to disappearance of Na_2WO_4 phase in the MnNaW-S/SiO_2 sample which, probably, can be the reason for worsening in the its catalytic properties (Fig. 2b). There are no sign of any additional phases in XRD pattern of these samples.

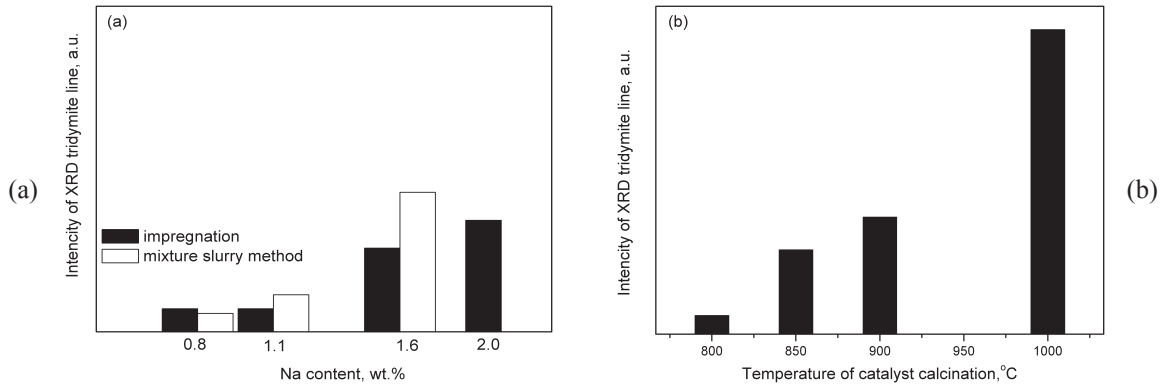

Fig. 9. Tridymite phase content vs. preparation condition: effect of Na content (a) and temperature of catalyst calcination (b).

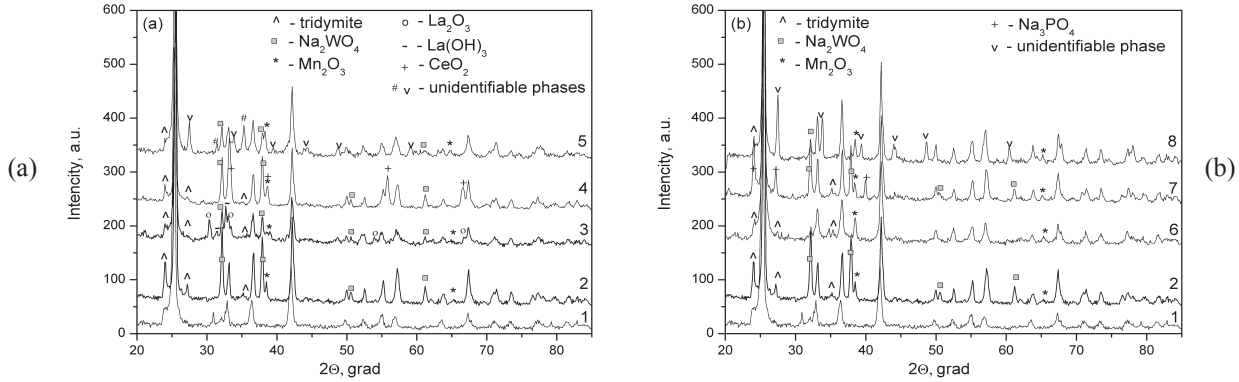

Fig. 10. Effect of promoter type on phase composition of MnNaW-X/SiO_2 catalysts. Calcination temperature is 850 ºC.(1) – α-cristobalite, (2) – 2Mn1.6Na3W/SiO_2, (3) – 2Mn1.6Na3W-5La/SiO_2, (4) – 2Mn1.6Na3W-5Ce/SiO_2, (5) – 2Mn1.6Na3W-3Zr/SiO_2, (6) – MnNaW-1S/SiO_2, (7) – 2Mn1.6Na3W-1P/SiO_2, (8) – 2Mn1.6Na3W-1Cl/SiO_2.

Figure 11 shows TEM typical images of SiO_2-based catalysts. As examples, fresh non-modified MnNaW/SiO_2 catalyst (Fig. 11a-c [17]) and La modified MnNaW-2La/SiO_2 catalysts (Fig. 11d-i) which are different by calcination temperature are examined. The 2Mn1.6Na3W/SiO_2 (I) catalyst prepared by impregnation consists of big globular SiO_2 particles of 5-10 μm. On the surface of SiO_2 support two kinds of particles are found: with high (1-2 nm, Fig. 11a,b) and rough (up to 50-100 nm, Fig. 11c) dispersion. According to the EDX data, the composition of particles of high dispersion is very variable and all supported metals (Mn, W and Na) are present in their composition. The particles of rough dispersion have mainly good cristallinity and different composition ($(Mn_2O_3)_3MnSiO_3$, MnO_x, WO_x/Na_2WO_4). It is noted that Na_2WO_4 phase is present as a rule in the form of an amorphous compound, on the surface of which small WO_3 crystallites are observed. It is probable that Na_2WO_4 phase is not stable under irradiation during TEM study, as it was previously shown for $Gd_2(WO_4)_3$ [32]. Concerning the 2Mn1.6Na3W/SiO_2 (M) catalyst prepared by the mixture slurry method, it consists of globular SiO_2 particles 0.5-0.6 μm in size. In other respects this sample resembles the MnNaW/SiO_2 (I) sample.

La introduction leads to the formation of crystallized bimetallic oxide particles (La-Mn-O, La-W-O) of 50-500 nm size (Fig. 11e,f [17]). There are also particles of high dispersion (Fig. 11d) as well as individual oxides (MnO_x and WO_x) which are observed in non-modified sample. At low La content (0.5 wt.%) $(Mn_2O_3)_3MnSiO_3$ (up to 50 nm) and WO_3 (0.5-2 nm) particles are main supported species. At an increase of La content up to 5 wt.% or an increase of temperature of catalyst calcination, in addition to $(Mn_2O_3)_3MnSiO_3$ and WO_3, particles of mixed oxide La-Mn-Si-O (as an example, $La_4Mn(Si_2O_7)_2(Mn_2O_4)_2$) and La-Si-O (as an example, $La_2Si_2O_7$) species are observed (Fig. 11g), which confirms strong interaction between metals and silica support. The crystalline phases of particles detected on the SiO_2 support by HRTEM do not exactly correspond to the phase compositions detected by XRD. In particular, $(Mn_2O_3)_3MnSiO_3$ and $La_4Mn(Si_2O_7)_2(Mn_2O_4)_2$ phases are not observed by XRD (Fig. 9). Nevertheless, according to TEM data these phases are present in all La-containing samples. Plausible reasons are: i) the particles have dimensions below the detection limit of XRD (ca. 3 nm); ii) low phase content; iii) complex XRD pattern of multicomponent materials in which some individual compounds have identical reflections.

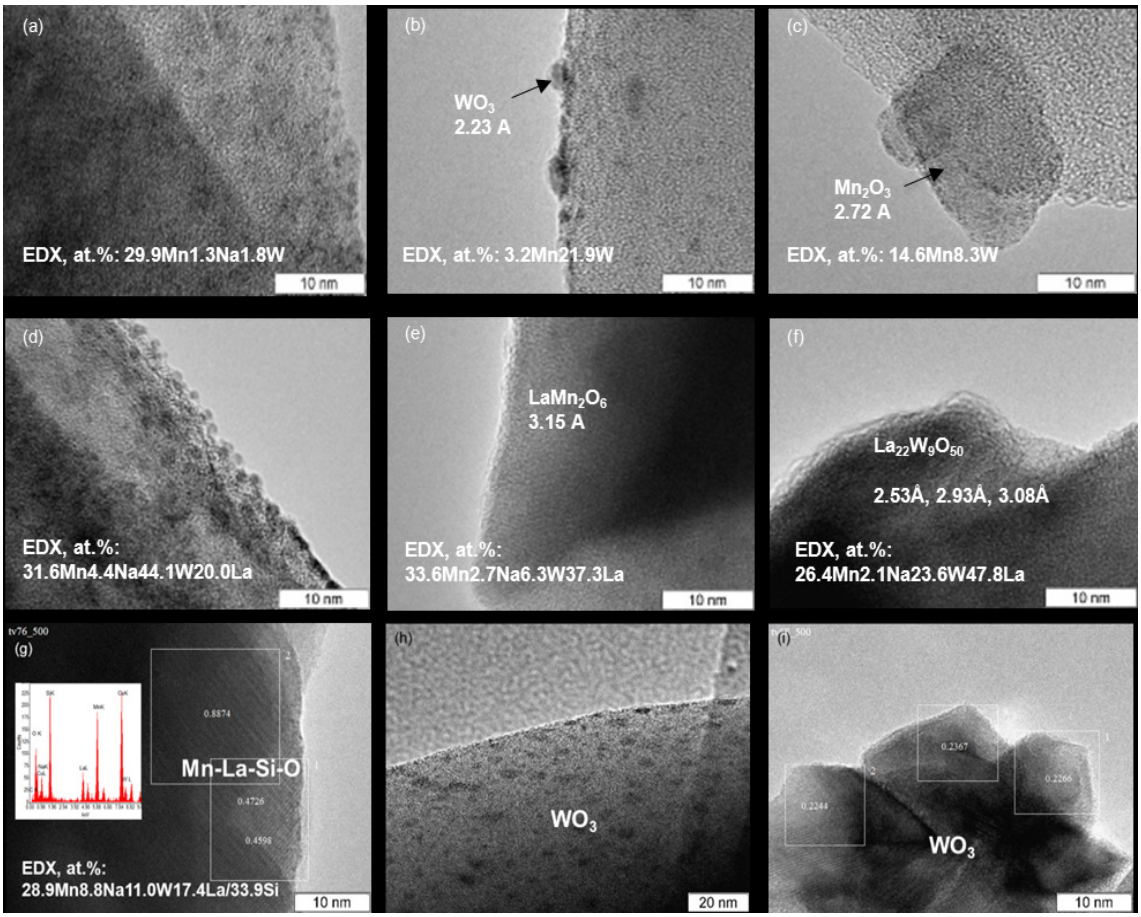

Fig. 11. TEM images of as-prepared 2Mn1.6Na3W/SiO_2 (I) after calcination at 850 ºC (a-c) [17], 2Mn1.6Na3.1W/-2La/SiO_2 (I) after calcination at 850 ºC (d-f) [17], 2Mn1.6Na3.1W/-2La/SiO_2 (I) catalysts after calcination at 1000 ºC (g-i).

The metal dispersion and distribution across the support in catalysts was estimated from XPS data. In case of MnNaW-2La/SiO_2 sample prepared by impregnation the surface Mn : Si, Na : Si, W : Si and La : Si ratios are higher than the bulk ratios, denoting that the metals reside preferentially on the silica surface than in the bulk (Table 4). This effect is more pronounced for Na. In case of MnNaW-2La/SiO_2 sample prepared by the mixture slurry method the surface Mn : Si, W : Si and La : Si ratio is close to the bulk ratio. So, as follows from XPS data, the mixture slurry method instead of the impregnation method provides more uniform distribution of Mn and W supported species across the SiO_2 matrix.

Figure 12b indicates that the chemical states of Mn are similar in all studied samples. The Mn 2p binding energy of 641.6 ± 0.1 eV is characteristic of the Mn^{3+} oxidation state on the surface [33, 34]. Na 1s peak at 1071.8 ± 0.1 eV observed by XPS indicates the Na^{+1} state [35]. The analysis of W 4f spectra shows BE = 35.6 ± 0.1 eV expected for W^{6+} [36, 37], and the spectra of different catalysts are similar to each other. It is not possible to distinguish WO_3 and Na_2WO_4 phases by XPS because of identical W^{6+} state in both phases [37]. Thus, the data of XPS demonstrates that preparation mode and temperature of calcinations doesn't affect the electronic states of MnNaW/SiO_2 catalyst components on the surface, while it significantly influences the distribution of active species across the support.

Table 4
Surface (XPS) and bulk (ICP, XFS) atomic ratios for 2Mn1.6Na3W-2La/SiO_2 catalysts

Preparation mode	Mn/Si		Na/Si		W/Si		La/Si	
	Surface	Bulk	Surface	Bulk	Surface	Bulk	Surface	Bulk
impregnation	0.05	0.03	0.20	0.03	0.03	0.01	0.03	0.01
mixture slurry method	0.03	0.03	0.17	0.05	0.014	0.012	0.01	0.01

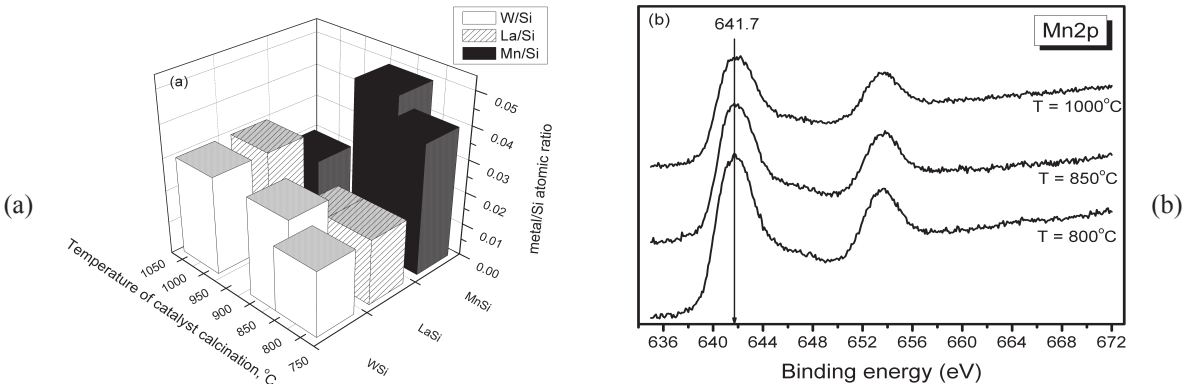

Fig. 12. Surface metal/Si atomic ratio (a) and XPS spectra in the Mn 2p (b) regions of the 2Mn1.6Na3W-2La/SiO_2 fresh catalysts: effect of temperature of catalyst calcination.

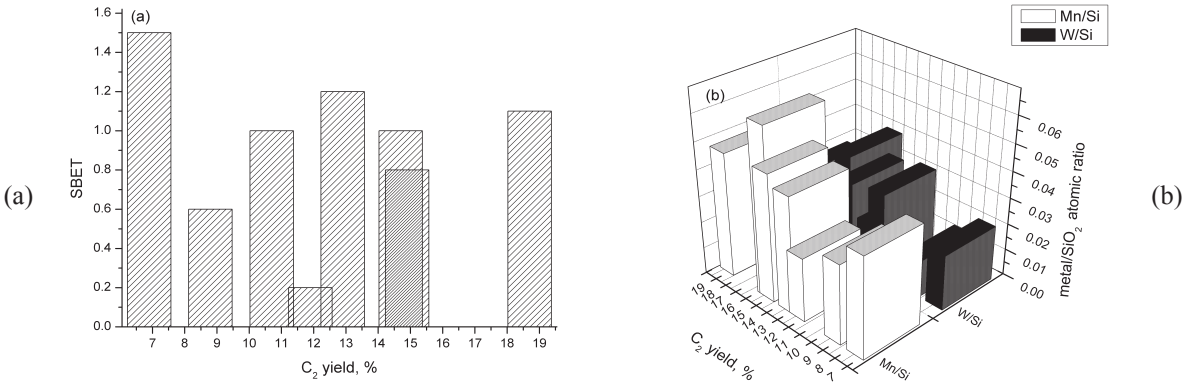

Fig. 13. Textural characteristics (a) and surface atomic ratio metal/SiO_2 (b) of 2Mn1.6Na3W-La/SiO_2 catalysts vs. their performance in OCM reaction.

As rule, for the OCM reaction, as an example of homogeneous-heterogeneous reaction, large surface areas and small particle sizes of catalyst are not beneficial [30, 38, 39]. Figure 13 a shows that variation of S_{BET} in the range 0.2-1.2 has practically no effect on the C_2 yield in the OCM reaction over 2Mn1.6Na3W-La/SiO_2 catalysts. Consequently, in this case, a correlation between the activity of a catalyst and its specific surface area was absent, and the catalytic properties of the samples were primarily caused by their phase composition, the state and surface concentration of metals, and the redox properties of the catalysts.

It is demonstrated that the Mn^{3+} is found as a proper oxidation state in the OCM reaction responsible for the methane activation [27, 40], and oxidized state of catalyst is necessary to maintain high C_2 selectivity [11]. Our XPS data confirm this observation (Fig. 13b): at an increase of Mn^{3+}/Si and W^{6+}/Si surface molar ratio the C_2 yield tends to increase. It is expected that the stability of OCM catalyst against deactivation should be related with stability of surface composition of catalyst during the OCM reaction. So the introduction of La seemingly leads to the stabilization of metal/Si atomic surface ratio and provides stable catalyst performance in the OCM reaction (Fig. 3). While the low activity of the catalyst which was calcined at 1000 ºC is mainly connected with the decrease of Mn/Si surface concentration (Fig. 4, 12a, 13b).

All these results clearly confirm that the MnNaW/SiO_2 catalyst performance in the OCM process can be regulated by the catalyst nanostructure design through variation of the catalyst preparation mode, temperature of calcination and introduction of cationic or anionic additives. At present it is difficult to unambiguously establish exactly which of the studied properties (phase composition, dispersion and distribution of supported metal-containing species) has a crucial influence on the catalyst performance. Further investigation of the effects of SiO_2 morphology and red-ox properties on the performance of silica-based catalyst in the OCM reaction is required and these topics are the subject of our current study.

3.2.2. LaSr/CaO

Table 5 shows main characteristics of LaSr/CaO catalysts which were prepared at variation of chemical composition and preparation method (physical

mixing (PM), citrate sol-gel method (S)). The catalysts prepared by the sol-gel method have a higher value of SBET than those for catalysts prepared by the physical mixing method. The specific surface area increases in the order: CaO (PM) ≈ 20Sr/CaO (PM) < 20La/CaO (PM) < 15La15Sr/CaO (PM) and CaO (S) ≈ 20Sr/CaO (S) < 15La-15Sr/CaO (S) ≈ 20La/CaO (S). Thus La adding to CaO led to a growth of the specific surface area of the LaSr/CaO samples. The modification of La/CaO catalysts by Na (0.5–1.5 wt.%.) has no influence on the phase composition of samples, but leads to a considerable decrease of specific surface area (from 11.5 to 2.5 m^2/g). According to XRD data, the CaO phase is the main phase of the prepared samples. For two-component systems with La (~20 wt.%), in addition of CaO phase the formation of La_2O_3 phase (JCPDS 5-602) occurs. It is noted that for 20La/CaO (S) sample, in contrast to 20La/CaO (PM) sample, trace amount of $La(OH)_3$ phase (JCPDS 36–1481) is detected. Probably, it is related to higher S_{BET} of 20La/CaO (S) sample in comparison with 20La/CaO (PM) sample. In the former case larger surface area provides higher interaction rate between La_2O_3 and water and, consequently, formation of $La(OH)_3$. For catalysts with Sr (~20 wt.%), the type of Sr-containing phase depends on the preparation method: SrO (JCPDS 6–520) is detected in case of 20Sr/CaO (PM) sample, while $SrCO_3$ (JCPDS 5–418) in case of 20Sr/CaO (S) sample. One can see from Table 6 that surface atomic ratios of 20La/CaO (PM) and 20La/CaO (S) fresh catalysts are different. The Ca surface concentration for 20La/CaO (S) catalyst is considerably higher than that for 20La/CaO (PM) catalyst, which is probably controlled by the preparation method. However the values of La surface concentration are the same for the both samples (Table 6).

According to TEM study, the fresh 20La/CaO (S) catalyst consists of big aggregates (~ 1 μm) of CaO and La_2O_3 particles of 50-200 nm size (Fig. 14). There are also small CaO particles 50 nm in size and region of oxide interfaces.

Thus, it is shown that for the LaSr/CaO catalysts the preparation method determines both value of specific surface area, surface and phase compositions. According to the mechanism of the reaction [30], the active oxygen species ZO_s (O^-, O_2^{2-}) on the catalyst surface are necessary for methane activation. The formation of active oxygen centers by means of substitution of regular cations M^{n+} of oxide lattice by other cations $M_1^{[n-1]+}$ is one of the approaches for developing active and stable OCM catalysts. So the growth of catalytic performance in the order: 20Sr/CaO (S) < 15La15Sr/CaO (S) < 20La/CaO can be explained by the increase of La^{3+} (against Sr^{2+}) content and, consequently, concentration of active oxygen species. This question has not been thoroughly investigated and will be studied in our next work. It is also expected that in case of La/CaO (S) catalyst prepared by the sol-gel method demonstrating higher catalytic activity in comparison to La/CaO (PM) catalyst prepared by the physical mixture method, the higher substitution degree of regular cations of oxide is realized because of intimate contact between oxides precursors at the stage of sol preparation.

Table 5
Characteristics of La-Sr/CaO catalysts: effect of chemical composition and preparation method

Sample	XRD data	Chemical composition, wt. %			S_{BET}, m^2/g	V_{pore}, cm^3/g	Average pore diameter, Å
		La	Sr	Ca			
20La/CaO (PM)	CaO, La_2O_3	19.6	-	47.8	1.4	0.005	140
20La/CaO (S)	CaO, La_2O_3, $La(OH)_3$	21.0	-	56.1	11.5	0.0039	137
15La15Sr/CaO (PM)	CaO, La_2O_3, SrO	14.0	12.1	47.6	2.7	0.010	139
15La15Sr/CaO (S)	CaO, La_2O_3, $SrCO_3$	16.1	13.7	50.1	12.0	0.056	186
20Sr/CaO (PM)	CaO, SrO	-	17.2	59.0	1.0	0.004	153
20Sr/CaO (S)	CaO, $SrCO_3$	-	17.6	58.4	5.9	0.018	125

Table 6
XPS Si 2p, Ca 2p and La 3d binding energies (eV) and surface atomic ratios of 20La/CaO (S) and 20La/CaO (PM) fresh catalysts

Sample	Binding energy (eV)			Surface atomic ratio	
	Si 2p3/2	Ca 2p3/2	La 3d5/2	Ca/Si	La/Si
20La/CaO (S)	103.3	347.1 (Ca^{2+})	835.5, 838.7 (La^{3+})	0.843	0.092
20La/CaO (PM)	103.3	346.8 (Ca^{2+})	835.2, 838.5 (La^{3+})	0.164	0.103

(a) 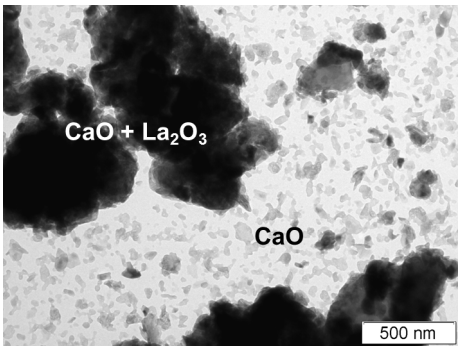

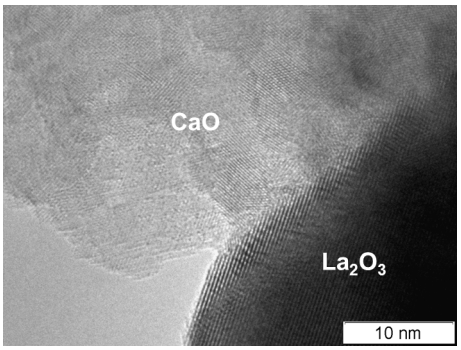

(b)

Fig. 14. TEM images of 20La/CaO (S) catalyst after calcinations at 850 ºC (a, b).

4. Conclusions

Representative series of OCM catalysts have been prepared and studied by a complex of physical-chemical methods. It was found that precise regulation of C_2 product yields in the OCM reaction could be achieved by appropriate variation of composition and preparation conditions of catalysts. The most perspective formulae of OCM catalysts were selected and the rational procedure of their synthesis was developed. High activity of 20La/CaO (prepared by the sol-gel method) and 2Mn1.6Na3.1W-2La/SiO_2 (prepared by the impregnation) determines prospective application of these catalysts in a catalytic membrane reactor, which seems really promising in further OCM studies. Presently, a prototype OCM membrane reactor is being built by our DEMCAMER project partners (HyGear B.V., the Netherlands, VITO, Belgium). The reactor will be tested with the developed OCM catalyst, and the results of the membrane reactor tests will be a topic of the next publication.

Acknowledgements

The authors are thankful to Dr. V.A. Ushakov, T.Ya. Efimenko, I.L. Kraevskaya, Dr. E.Yu. Gerasimov (all from the Boreskov Institute of Catalysis) for their assistance with catalyst characterization.

The presented research was initiated by European Union 7th Framework Programme (FP7/2007–2013) under grant agreement No. 262840 and has received funding from Russian Federal Agency of Scientific Organizations (V45-1-10).

References

[1]. Z.R. Ismagilov, E.V. Matus and L.T. Tsikoza, Energy Environmental Science 5 (2008) 526–541.
[2]. S. Arndt, T. Otremba, U. Simon, M. Yildiz, H. Schubert and R. Schomacker, Appl. Catal. A: General 53 (2012) 425–426.
[3]. I.Z. Ismagilov, E.V. Matus, V.V. Kuznetsov, N. Mota, R.M. Navarro, M.A. Kerzhentsev, Z.R. Ismagilov, J.L.G. Fierro, Catal. Today 210 (2013) 10–18.
[4]. I.Z. Ismagilov, E.V. Matus, V.V. Kuznetsov, N. Mota, R.M. Navarro, S.A. Yashnik, I.P. Prosvirin, M.A. Kerzhentsev, Z.R. Ismagilov, J.L.G. Fierro, Appl. Catal. A: General 481 (2014) 104–115.
[5]. I.Z. Ismagilov, E.V. Matus, V.V. Kuznetsov, M.A. Kerzhentsev, S.A. Yashnik, I.P. Prosvirin, N. Mota, R.M. Navarro, J.L.G. Fierro, Z.R. Ismagilov, Int. J. Hydrogen Energy 39 (2014) 20992–21006.
[6]. E.V. Matus, I.Z. Ismagilov, O.B. Sukhova, V.I. Zaikovskii, L.T. Tsikoza, Z.R. Ismagilov, J.A. Moulijn, Industrial Engineering Chemistry Research 46 (2007) 4063–4074.
[7]. E.V. Matus, O.B. Sukhova, I.Z. Ismagilov, L.T. Tsikoza, Z.R. Ismagilov, React. Kinet. Catal. Lett. 98 (2009) 59–67.
[8]. U. Zavyalova, M. Holena, R. Schlogl and M. Baerns, ChemCatChem 3 (2011) 1935–1947.
[9]. Z.R. Ismagilov, A. Parmaliana, F. Frusteri, D. Miceli, A.A. Kirchanov, G.B. Barannik, Catal. Today 24 (1995) 281–284.
[10]. S. Pak, P. Qiu and J.H. Lunsford, J. Catal. 179 (1998) 222–230.
[11]. T.P. Tiemersma, M.J. Tuinier, F. Gallucci, J.A.M. Kuipers and M. van Sint Annaland, Appl. Catal. A: General 96 (2012) 433–434.
[12]. S. Jaso, S. Sadjadi, H.R. Godini, U. Simon, S. Arndt, O. Gorke, A. Berthold, H. Arellano-Garcia, H. Schubert, R. Schomacker and G. Wozny, Journal of Natural Gas Chemistry 21 (2012) 534–543.
[13]. S. Bhatia, C.Y. Thien and A.R. Mohamed, Chem. Eng. J. 148 (2009) 525–532.
[14]. X. Dong, W. Jin, N. Xu and K. Li, Chem. Commun. 47 (2011) 10886–10902.
[15]. O. Czuprat, T. Schiestel, H. Voss and J. Caro, Industrial & Engineering Chemistry Research 49 (2010) 10230–10236.

[16]. Y. Wei, W. Yang, J. Caro and H. Wang, Chem. Eng. J. 220 (2013) 185–203.
[17]. I.Z. Ismagilov, E.V. Matus, V.V. Kuznetsov, S.D. Vasil'ev, M.A. Kerzhentsev, Z.R. Ismagilov, Kinet. Catal., 2015, 56, No. 4, 459.
[18]. J.H. Scofield, J. Electron. Spectrosc. Relat. Phenom. 8 (1976) 129–137.
[19]. S. Pak, J.H. Lunsford, Appl. Catal. A: General 168 (1998) 131–137.
[20]. D.J. Wang, M.P. Rosynek, J.H. Lunsford, J. Catal. 155 (1995) 390–402.
[21]. J.S. Ahari, M.T. Sadeghi, S. Zarrinpashne, Journal of Natural Gas Chemistry 20 (2011) 204–213.
[22]. L. Wang, L. Chou, B. Zhang, H. Song, J. Zhao, J. Yang, S. Li, J. Mol. Catal. A: Chem. 245 (2006) 272–277.
[23]. X. Wang, S. Li, Shiyou Huagong, 1997, 26, 381.
[24]. Y.T. Chua, A.R. Mohamed, S. Bhatia, Appl. Catal. A: General 343 (2008) 142–148.
[25]. L. Chou, Y. Cai, B. Zhang, J. Niu, S. Ji, S. Li, Journal of Natural Gas Chemistry, 2002, 11, 131.
[26]. M.R. Ehsani, S.M. Ghoreishi, Industrial Engineering Chemistry Research 16 (2010) 923–928.
[27]. W. Zheng, D. Cheng, F. Chen and X. Zhan, Journal of Natural Gas Chemistry 19 (2010) 515–521.
[28]. L.M. Ioffe, P. Bosch, T. Viveros, H. Sanchez, Y.G. Borodko, Mater. Chem. Phys. 51 (1997) 269–275.
[29]. V. Salehoun, A. Khodadadi, Y. Mortazavi, A. Talebizadeh, Chem. Eng. Sci. 63 (2008) 4910–4916.
[30]. V.S. Arutunov, and O.V. Krylov, Oxidative conversion of methane, 1998, Moscow: Nauka.
[31]. Sinev, M.A., Doctoral (Chem) Dissertation, Moscow: Semenov Institute of Chemical Physics, 2011.
[32]. Y. Zeng, Z. Li, L. Wang and Y. Xiong, CrystEngComm 14 (2012) 7043–7048.
[33]. B.R. Strohmeier and D.M. Hercules, J. Phys. Chem. 88 (1984) 4922–4929.
[34]. V.B. Bayer, R. Podloucky and C. Franchini, Phys. Rev. B: Condens. Matter. 76 (2007) 165428-1 – 165428-10.
[35]. C.D. Wagner, Faraday Discussions of the Chemical Society 60 (1975) 291–300.
[36]. S.C. Moulzolf, S. Ding and R.J. Lad, Sensors and Actuators B, 77 (2001) 375–382.
[37]. S.F. Ho, S. Contarini and J.W. Rabalais, Phys. Chem. 91 (1987) 4779–4788.
[38]. M. Gharibi and F.T. Zangeneh, F. Yaripour and S. Sahebdelfar, Appl. Catal. A: General 8 (2012) 443–444.
[39]. K. Langfeld, B. Frank, V.E. Strempel, C. Berger-Karin, G. Weinberg, E.V. Kondratenko and R. Schomäcker, Appl. Catal. A: General 417-418 (2012) 145–152.
[40]. S. Hou, Y. Cao, W. Xiong, H. Liu and Y. Kou, Industrial and Engineering Chemistry Research 45 (2006) 7077–7083.